

MIT Open Access Articles

Planet-induced Stellar Pulsations in HAT-P-2's Eccentric System

The MIT Faculty has made this article openly available. **Please share** how this access benefits you. Your story matters.

Citation: Wit, Julien de; Lewis, Nikole K.; Knutson, Heather A.; Fuller, Jim; Antoci, Victoria; Fulton, Benjamin J. and Laughlin, Gregory et al. "Planet-Induced Stellar Pulsations in HAT-P-2's Eccentric System." *The Astrophysical Journal* 836, no. 2 (February 2017): L17 © 2017 The American Astronomical Society

As Published: <http://dx.doi.org/10.3847/2041-8213/836/2/L17>

Persistent URL: <http://hdl.handle.net/1721.1/110154>

Version: Final published version: final published article, as it appeared in a journal, conference proceedings, or other formally published context

Terms of Use: Article is made available in accordance with the publisher's policy and may be subject to US copyright law. Please refer to the publisher's site for terms of use.





Planet-induced Stellar Pulsations in HAT-P-2's Eccentric System

Julien de Wit¹, Nikole K. Lewis², Heather A. Knutson³, Jim Fuller^{4,5}, Victoria Antoci⁶, Benjamin J. Fulton^{7,17}, Gregory Laughlin⁸, Drake Deming⁹, Avi Shporer^{10,18}, Konstantin Batygin³, Nicolas B. Cowan¹¹, Eric Agol¹², Adam S. Burrows¹³, Jonathan J. Fortney¹⁴, Jonathan Langton¹⁵, and Adam P. Showman¹⁶

¹ Department of Earth, Atmospheric and Planetary Sciences, MIT, 77 Massachusetts Avenue, Cambridge, MA 02139, USA

² Space Telescope Science Institute, 3700 San Martin Drive, Baltimore, MD 21218, USA

³ Division of Geological and Planetary Sciences, California Institute of Technology, Pasadena, CA 91125, USA

⁴ TAPIR, Walter Burke Institute for Theoretical Physics, Mailcode 350-17, California Institute of Technology, Pasadena, CA 91125, USA

⁵ Kavli Institute for Theoretical Physics, University of California, Santa Barbara, CA 93106, USA

⁶ Stellar Astrophysics Centre, Department of Physics and Astronomy, Aarhus University, Ny Munkegade 120, DK-8000 Aarhus C, Denmark

⁷ Institute for Astronomy, University of Hawaii, Honolulu, HI 96822, USA

⁸ Department of Astronomy, Yale University, New Haven, CT 06511, USA

⁹ Department of Astronomy, University of Maryland at College Park, College Park, MD 20742, USA

¹⁰ Jet Propulsion Laboratory, California Institute of Technology, 4800 Oak Grove Drive, Pasadena, CA 91009, USA

¹¹ Department of Physics, Department of Earth and Planetary Sciences, McGill University, 3550 rue University, Montreal, QC H3A 2A7, Canada

¹² Department of Astronomy, University of Washington, Seattle, WA 98195, USA

¹³ Department of Astrophysical Sciences, Princeton University, Princeton, NJ 08544, USA

¹⁴ Department of Astronomy and Astrophysics, University of California, Santa Cruz, CA 95064, USA

¹⁵ Department of Physics, Principia College, Elsah, IL 62028, USA

¹⁶ Lunar and Planetary Laboratory, University of Arizona, Tucson, AZ 85721, USA

Received 2016 December 14; revised 2017 January 11; accepted 2017 January 12; published 2017 February 14

Abstract

Extrasolar planets on eccentric short-period orbits provide a laboratory in which to study radiative and tidal interactions between a planet and its host star under extreme forcing conditions. Studying such systems probes how the planet's atmosphere redistributes the time-varying heat flux from its host and how the host star responds to transient tidal distortion. Here, we report the insights into the planet–star interactions in HAT-P-2's eccentric planetary system gained from the analysis of ~ 350 hr of $4.5 \mu\text{m}$ observations with the *Spitzer Space Telescope*. The observations show no sign of orbit-to-orbit variability nor of orbital evolution of the eccentric planetary companion, HAT-P-2 b. The extensive coverage allows us to better differentiate instrumental systematics from the transient heating of HAT-P-2 b's $4.5 \mu\text{m}$ photosphere and yields the detection of stellar pulsations with an amplitude of approximately 40 ppm. These pulsation modes correspond to exact harmonics of the planet's orbital frequency, indicative of a tidal origin. Transient tidal effects can excite pulsation modes in the envelope of a star, but, to date, such pulsations had only been detected in highly eccentric stellar binaries. Current stellar models are unable to reproduce HAT-P-2's pulsations, suggesting that our understanding of the interactions at play in this system is incomplete.

Key words: methods: numerical – planet–star interactions – planets and satellites: atmospheres – planets and satellites: dynamical evolution and stability – planets and satellites: individual (HAT-P-2b) – techniques: photometric

1. Introduction

Owing to its large mass ($8 M_{\text{Jup}}$), short orbital period ($P \sim 5.63$ day), and eccentricity ($e \sim 0.5$), the hot Jupiter HAT-P-2 b (Bakos et al. 2007) is a favored target for the study of planet–star interactions (Fortney et al. 2008; Jordan & Bakos 2008; Langton & Laughlin 2008; Fabrycky & Winn 2009; Levrard et al. 2009; Hartman 2010; Cowan & Agol 2011; Cébron et al. 2013; Kataria et al. 2013; Lewis et al. 2013, 2014; Salz et al. 2016). Measurements of the flux variations caused by its transient heating obtained at 3.6 , 4.5 , and $8.0 \mu\text{m}$ with *Spitzer* yielded the first insights into the planet's response to transient heating (Lewis et al. 2013) but were not reproducible by atmospheric models (Lewis et al. 2014), in particular at $4.5 \mu\text{m}$. Here, we present the analysis of all the observations of HAT-P-2 b obtained at $4.5 \mu\text{m}$ with *Spitzer*—including 2 new primary and 16 new secondary eclipses—whose extensive coverage allows us to better

differentiate instrumental systematics from the transient heating of HAT-P-2 b's $4.5 \mu\text{m}$ photosphere and yields the detection of unexpected pulsations with an amplitude of 40 ppm.

2. Observations and Analysis

The observations total 350 hr (2.9 million 32×32 pixels subarray images with a 0.4 s exposure time) and include (1) a full-orbit phase curve obtained between 2011 July 9 and 15 (Lewis et al. 2013), (2) 16 new secondary eclipses—including 2 partial phase curves each covering 30 hr post-periastron passage—obtained between 2013 April and October (PI: H. Knutson), and (3) 2 new primary and 2 new secondary eclipses obtained between 2015 October and November (PI: N. Lewis).

We extract the photometry following the method detailed in de Wit et al. (2016). While Lewis et al. (2013) used a fixed aperture of 2.25 pixels to minimize the scatter in the final solution, we use here for all the Astronomical Observation Requests (AORs) time-varying apertures with a radius equal to the square root of the noise-pixel parameter $\tilde{\beta}$ (see, e.g., Mighell 2005; Lewis et al. 2013) with an AOR-dependent

¹⁷ NSF Graduate Research fellow.

¹⁸ Sagan Postdoctoral fellow.

Table 1
Description of HAT-P-2's AOR^a at 4.5 μm

AORKEY(\oplus^b)	Start Time [UT]	Eclipse Time [BJD-2455000]	Eclipse Depth [p.p.m]	Pulsation Amplitude [p.p.m.]	Aperture ^c [px]	β_{red}^d
42789632(O)	2011 Jul 9 1:51	5751.8763 \pm 0.0012	1120 \pm 83	36 \pm 90	$\sqrt{\tilde{\beta}}$ -0.6 (2.1)	1.55
42789888(P)	2011 Jul 10 1:36	$\sqrt{\tilde{\beta}}$ -0.6 (1.9)	1.4
43962624(P)	2011 Jul 11 3:16	$\sqrt{\tilde{\beta}}$ -0.6 (1.9)	1.2
43962880(P)	2011 Jul 12 3:01	$\sqrt{\tilde{\beta}}$ -0.6 (2.1)	1.5
43963136(T)	2011 Jul 13 2:12	5756.42696 \pm 0.00047	4961 \pm 72	12 \pm 42	$\sqrt{\tilde{\beta}}$ -0.6 (1.9)	1.4
43963392(O)	2011 Jul 14 1:56	5757.5081 \pm 0.0013	1116 \pm 117	32 \pm 83	$\sqrt{\tilde{\beta}}$ -0.6 (1.8)	1.45
46473216(O)	2013 Oct 31 4:49	6394.0922 \pm 0.0014	839 \pm 93	-56 \pm 56	$\sqrt{\tilde{\beta}}$ -0.5 (1.7)	1.15
46473472(O)	2013 Oct 19 22:45	6422.2591 \pm 0.0016	858 \pm 97	76 \pm 46	$\sqrt{\tilde{\beta}}$ -0.5 (1.6)	1.6
46473728(O)	2013 Oct 14 7:21	6427.8928 \pm 0.0011	854 \pm 83	78 \pm 45	$\sqrt{\tilde{\beta}}$ -0.5 (1.5)	1.05
46474496(O)	2013 Sep 21 18:24	6489.8599 \pm 0.0013	887 \pm 96	-16 \pm 45	$\sqrt{\tilde{\beta}}$ -0.4 (2.1)	1.55
46474752(O)	2013 Sep 16 3:11	6495.4952 \pm 0.0015	899 \pm 110	39 \pm 49	$\sqrt{\tilde{\beta}}$ -0.6 (1.8)	1.2
46475008(O)	2013 Aug 30 5:55	6529.2941 \pm 0.0014	1002 \pm 96	99 \pm 42	$\sqrt{\tilde{\beta}}$ -0.5 (1.55)	1.3
46475264(O)	2013 Aug 24 14:26	6534.9295 \pm 0.0013	959 \pm 86	20 \pm 41	$\sqrt{\tilde{\beta}}$ -0.6 (1.45)	1.4
46475520(O)	2013 Jul 21 19:19	6540.5602 \pm 0.0010	802 \pm 97	96 \pm 49	$\sqrt{\tilde{\beta}}$ -0.7 (1.6)	1.3
46475776(O)	2013 Jul 16 4:21	6551.8272 \pm 0.0012	974 \pm 84	7 \pm 43	$\sqrt{\tilde{\beta}}$ -0.5 (1.5)	1.15
46476032(O)	2013 May 15 4:55	6557.4625 \pm 0.0011	987 \pm 90	37 \pm 41	$\sqrt{\tilde{\beta}}$ -0.6 (1.45)	1.2
46476288(O)	2013 May 9 13:53	6579.9946 \pm 0.0010	901 \pm 88	69 \pm 39	$\sqrt{\tilde{\beta}}$ -0.5 (1.55)	1.45
46476544(O)	2013 Apr 11 9:42	6585.6294 \pm 0.0013	750 \pm 83	18 \pm 48	$\sqrt{\tilde{\beta}}$ -0.5 (1.55)	1.35
46477312(P)	2013 Sep 5 21:46	$\sqrt{\tilde{\beta}}$ -0.6 (1.55)	1.6
46477568(P)	2013 Sep 5 9:46	$\sqrt{\tilde{\beta}}$ -0.6 (1.45)	1.3
46477824(O)	2013 Sep 4 21:45	6591.2611 \pm 0.0010	890 \pm 80	94 \pm 40	$\sqrt{\tilde{\beta}}$ -0.5 (1.55)	1.2
46478336(P)	2013 Oct 26 14:45	$\sqrt{\tilde{\beta}}$ -0.5 (1.5)	1.2
46478592(P)	2013 Oct 26 2:45	$\sqrt{\tilde{\beta}}$ -0.4 (1.6)	1.2
46478848(O)	2013 Oct 25 14:44	6596.8941 \pm 0.0012	918 \pm 76	-20 \pm 38	$\sqrt{\tilde{\beta}}$ -0.5 (1.55)	1.4
57787136(T)	2015 Oct 21 13:20	7316.89688 \pm 0.00047	4923 \pm 66	-40 \pm 74	$\sqrt{\tilde{\beta}}$ -0.7 (1.35)	1.1
57786880(T)	2015 Nov 18 17:39	7345.06511 \pm 0.00051	4948 \pm 71	15 \pm 71	$\sqrt{\tilde{\beta}}$ -0.7 (1.4)	1.05
57787648(O)	2015 Nov 19 19:28	7346.1474 \pm 0.0012	102 \pm 99	19 \pm 68	$\sqrt{\tilde{\beta}}$ -0.5 (1.6)	1.45
57787392(O)	2015 Nov 25 10:49	7351.7813 \pm 0.0011	864 \pm 87	33 \pm 85	$\sqrt{\tilde{\beta}}$ -0.6 (1.4)	1.35

Notes.

^a AORs are composed of data sets (FITS files); each data set corresponds to 64 individual subarray images of 32×32 px. The exposure time was set to 0.4 s.

^b AORKEY target: T, O, or P respectively for transit, occultation, or phase curve measurements.

^c We optimize our choice of aperture individually for each AOR. We find that time-varying apertures equal to the square root of the noise-pixel parameter $\tilde{\beta}$ best reduce the scatter in the final time series. The average aperture radii are shown in parentheses.

^d The β_{red} coefficients are used to estimate the fraction of remaining time-correlated noise in our final time series and to account for it in our error estimates. To do so, we follow a procedure similar to Winn et al. (2008).

constant offset estimated to minimize the relative amount of red noise in the final time series of each AOR (see Table 1). The resulting aperture radius has an average across all AORs of 1.75 pixels. We trim outliers from the resulting time series for each visit, discarding 0.8% of the images overall.

As for the photometry extraction, we follow the standard procedures described in de Wit et al. (2016) to analyze the photometry, allowing us to reach photometric precisions of 75 ppm per 1 hr bin. We update the combined instrumental and astrophysical model to include functional forms to account for the transient heating of the planet's atmosphere due to its eccentric orbit and the stellar pulsations. The resulting phase-folded photometry is shown in Figure 1.

2.1. Nominal Model

We model transits and occultations following Mandel & Agol (2002) and allow the eclipse times to vary to search for

possible orbital evolution. We model HAT-P-2's transient heating using the functional forms introduced in Lewis et al. (2013). We find that the asymmetric Lorentzian function is favored over the function based on harmonics in orbital phase ($\Delta\text{BIC} = -7$). This difference is due to 2 new partial phase curves obtained after periastron passage together with 16 new occultations that provide a stronger leverage on HAT-P-2 b's flux modulation around occultation allowing a better disentanglement from the instrumental systematics.

2.2. Pixelation Effect and Intrapixel Sensitivity Variations

The change in position of the target's point-spread function (PSF) over a detector with non-uniform intrapixel sensitivity leads to apparent flux variations that are strongly correlated with the PSF position. We account for this effect using the same implementation of the pixel-mapping method as in Lewis

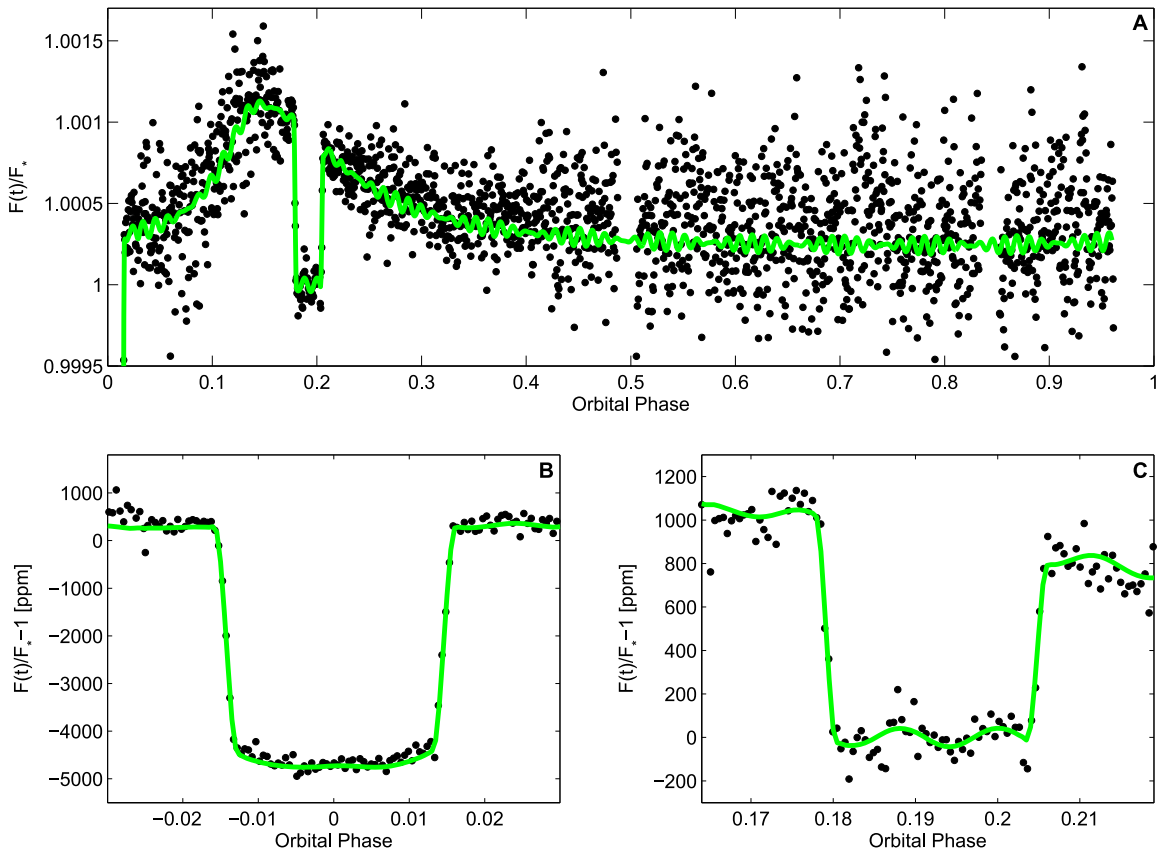


Figure 1. HAT-P-2 b’s photometry observed at $4.5 \mu\text{m}$. The photometry (black filled circles) combines ~ 350 hr of observations obtained between 2011 July 9 and 2015 November and includes 3 primary and 18 secondary eclipses. The photometry is presented normalized, with instrumental effects removed, phase-folded, and binned into intervals of 0.00025 in orbital phase—which corresponds to two-minute intervals. The decrease in data point spread around occultation and periastron passage is due to the multiple observations at these orbital phases. We overplot the best-fit model light curve in green. (A) Phase curve. (B) Transit. (C) Occultation.

et al. (2013)—see, e.g., Wong et al. (2015) and Ingalls et al. (2016) for detailed method comparisons.

2.3. Detector Ramp

IRAC observations often display an exponential increase in flux at the beginning of a new observation. The standard procedure for $4.5 \mu\text{m}$ observations is to trim the first hour at the start of each observation and subsequent downlinks, which reduces the complexity of fits with minimal loss of information on the eclipse shape and time (Lewis et al. 2013). However, we find here that the photometry around the primary and secondary eclipses shows a positive trend. Individual primary and secondary eclipse fits allowing for the correction of a linear trend in the photometry show that the trend is consistent across all epochs and has a slope of $65 \pm 6 \text{ ppm hr}^{-1}$ (see Table 1). Similarly to Stevenson et al. (2012), we find that this trend is best accounted for with a simple exponential function.

2.4. Pulsations

While fitting HAT-P-2’s photometry with the standard models introduced above, we observed additional signals in the photometry in the forms of oscillations (Figure 1). We account for the oscillations by including sine functions in our global fit—details in Sections 3.4 and 4.1.

2.5. Time-correlated Noise and Uncertainty Estimates

We find that the standard deviation of our best-fit residuals is a factor of 1.11 higher than the predicted photon noise limit at $4.5 \mu\text{m}$. We expect that this noise is most likely instrumental in nature and account for it in our error estimates using a scaling factor β_{red} for the measurement errorbars (Gillon et al. 2010). We find that the average β_{red} is 1.3, the maximum values corresponding to a timescale of ~ 50 minutes.

3. Results

3.1. Orbit-to-orbit Variability

We find no sign of variability across the 18 occultations obtained with *Spitzer* at $4.5 \mu\text{m}$. The occultation depths estimated via individual fits are shown in Figure 2(A) and are all consistent with the global-fit estimate within $\sim 1\sigma$. This implies that the thermal structure of HAT-P-2 b’s $4.5 \mu\text{m}$ photosphere around occultation shows no sign of orbit-to-orbit variability. This lack of significant orbit-to-orbit variability is consistent with the predictions presented in Lewis et al. (2014).

The reproducibility of the parameter estimates across 18 occultations obtained over 4 years also further emphasizes the reliability of current techniques used for the acquisition and analysis of Warm *Spitzer* measurements (see also, e.g., Wong et al. 2015, 2016; Ingalls et al. 2016).

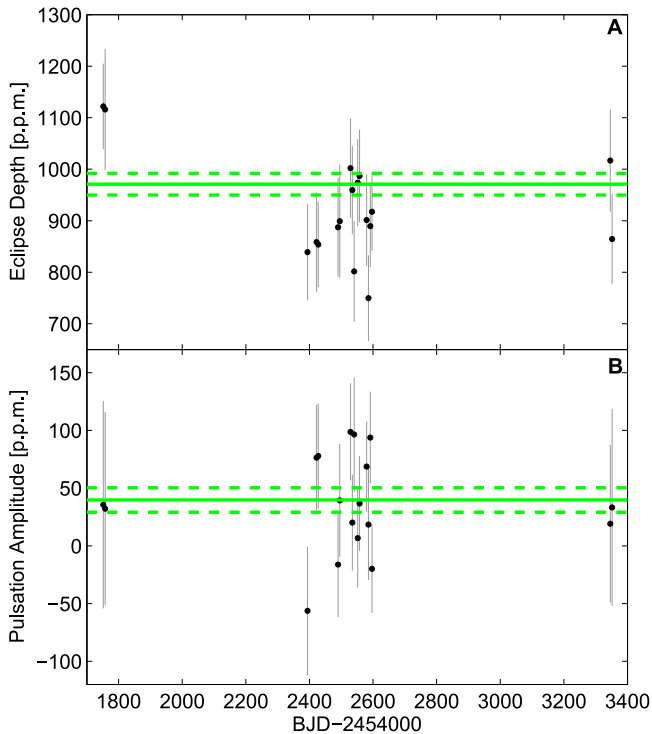


Figure 2. Estimates of occultation depth (A) and pulsation amplitude (B) for the 18 occultations observed in the $4.5\ \mu\text{m}$ *Spitzer* band (Table 1). (A) The green lines indicate the best-fit occultation depth and corresponding 1σ uncertainties from the global fit. The good agreement between the individual occultation depth estimates and the global fit implies no orbit-to-orbit variability for HAT-P-2 b’s $4.5\ \mu\text{m}$ photosphere and highlights the consistency of *Spitzer* measurements. (B) The individual amplitudes scatter homogeneously around 40 ppm. No single occultation can provide a significant detection of the pulsation signal due to noise limitations with a single observation. However, all the individual occultation amplitudes are consistent with the combined pulsation signal. The green lines indicate the mean of the individual fits and their standard deviation, which is in good agreement with each individual estimate.

3.2. HAT-P-2’s Orbital Parameters and Ephemeris

We find no sign of orbital evolution from the estimated times of primary and secondary eclipses (Table 1). We derive a new ephemeris from a simultaneous fit of our measured primary and secondary eclipse times, those from the literature (all but the $4.5\ \mu\text{m}$ eclipse times gathered in Lewis et al. 2013) and HAT-P-2’s radial velocity (RV) measurements¹⁹ (Table 1). Our new observations extend the previous baseline by a factor of two and the number of occultations by a factor of five yielding ultra-precise estimates of HAT-P-2 b’s orbital period, mid-transit time, orbital eccentricity, and argument of periastron:

$$\begin{aligned} P &= 5.6334675 \pm 1.3 \times 10^{-6} \text{ days} \\ T_{c,0} &= 2455288.84969 \pm 0.00039 \text{ BJD} \\ e &= 0.51023 \pm 0.00042 \\ \omega &= 188^\circ.44 \pm 0^\circ.43. \end{aligned} \quad (1)$$

Our global fit of HAT-P-2’s photometry also yields improved constraints on the transit depth (4941 ± 39 ppm), the occultation depth (971 ± 21 ppm, which translates into a hemisphere-averaged brightness temperature of 2182 ± 27 K), the orbital inclination ($86^\circ.16 \pm 0^\circ.26$), and stellar density

($0.434 \pm 0.020 \text{ g cm}^{-3}$). We also derive from the ultra-precise eclipse times the 3σ upper limit on the variation of HAT-P-2 b’s orbital eccentricity and argument of periastron, respectively, $0^\circ.0012$ and $0^\circ.90$ per year.

3.3. HAT-P-2 b’s Transient Heating

The extensive coverage of HAT-P-2 b’s occultation and post-periastron passage allows us to disentangle further systematics from the planetary flux modulation. The result is a phase curve (Figure 1) whose main difference with Lewis et al. (2013) is a lower minimum— 322 ± 69 ppm, which translates into a hemisphere-averaged temperature of 1327 ± 106 K. We find an excellent agreement on the timing and amplitude of the planetary flux peak, 5.40 ± 0.57 hr after periastron passage and 1178 ± 34 ppm—which translates into a hemisphere-averaged temperature of 2425 ± 40 K. The timescales for the planetary flux increase and decrease are respectively 5.5 ± 1.1 hr and 10.3 ± 1.5 hr. Because of the orbital geometry of HAT-P-2 b with periastron passage occurring midway between transit and occultation, the measured flux increase and decrease timescales are likely an overestimate of the true radiative timescale of HAT-P-2 b’s atmosphere near the $4.5\ \mu\text{m}$ photosphere, but are consistent with a short atmospheric radiative timescale of a few hours. The results presented here are in excellent agreement with the predictions from three-dimensional general circulation models presented in Lewis et al. (2014).

3.4. HAT-P-2’s Pulsations

Our analysis also reveals distinct pulsations with a period of approximately 87 minutes in HAT-P-2’s photometry (Figure 1). The oscillations are observed during the occultations, which implies that if they are astrophysical in nature they must originate from the host star and not the planet. We verify that the pulsations are not due to a strong instrumental signal in a subset of the AORs that would then be diluted by the inclusion of additional observations without this signal. We first explore this possibility by showing that the oscillations are consistently visible across subsets of AORs. To do so, we randomly picked off the 18 occultation AORs, 25 random sets of 9 AORs, 25 random sets of 5 AORs, and 25 random sets of 3 AORs and included in our model a sine function. We found that all but two of the sets of three AORs and one of five AORs yield a consistent detection of the pulsation. The consistency of the retrieved pulsation implies that, although the pulsation is not detectable from an individual AOR, the SNR of five AORs combined is sufficient to yield a $>2\sigma$ detection. Furthermore, its consistency over these different AOR subsets indicates its coherence. We explore this further by including a sine curve function in the model and allowing its amplitude to vary individually for each occultation AOR. We find that the individual amplitudes scatter around 40 ppm, while the significance of the pulsation detection in each individual visit is less than 1σ (Figure 2(B)). The pulsations are hence present in each individual occultation AOR, but its study requires fitting multiple AORs.

The transit photometry, however, shows no sign of such short-period oscillations (Figure 1(B) and Table 1). Similar individual fits lead to an oscillation amplitude of 3 ± 15 ppm in transit. The pulsations build coherently when we combine 18 distinct epochs of data, which implies that the pulsation is a harmonic of the planet orbital frequency, as shown by the periodogram of the

¹⁹ RV measurements obtained by the California Planet Search (CPS) team with the HIRES instrument (Vogt et al. 1994) on Keck using the CPS pipeline (Howard et al. 2009).

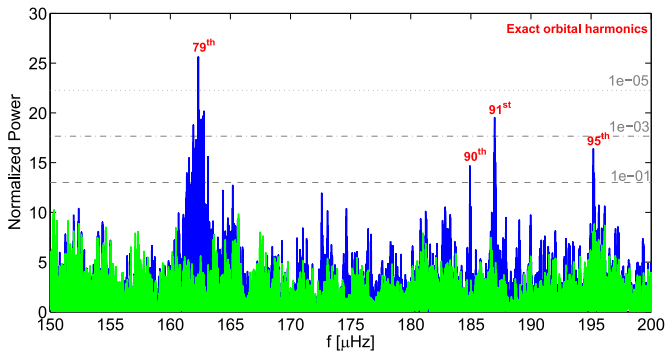


Figure 3. Periodogram of the 4.5 micron photometry after subtracting the best-fit model. The periodogram prior to accounting for the pulsations is shown in blue and the periodogram of the residuals after the best-fit pulsation model has been removed is shown in green. Significance levels are expressed in terms of false-positive probability via horizontal gray lines.

residuals (Figure 3). The two most significant peaks correspond to HAT-P-2 b’s 79th and 91st orbital harmonics, which are found to interfere constructively around occultations but destructively around transits as a result of the relative phase of the two harmonics. The pulsations are therefore astrophysical in nature unless the instrumental systematics appear to be harmonics of HAT-P-2 b’s orbital frequency phased in such a way that they build coherently over all the different epochs. This scenario would require that the modulation of the detector gain/noise or the PSF position/shape²⁰ follows a repeated pattern of oscillatory changes that are not only harmonics of the planet’s orbital frequency, but also constructively phased. We use the noise-pixel parameter (Mighell 2005; Lewis et al. 2013) as a proxy for any changes in the PSF position and shape. We use the “sky” background as a proxy for gain variations and electronic noise. We find that the periodograms of the PSF position (Figures 4(B) and (C)) and of the noise-pixel parameter (Figure 4(D)) show no significant peak in the period range related to the pulsations while showing a significant signal at *Spitzer*’s pointing oscillation period. Similarly, the periodogram of the “sky” background shows no specific peak around the 79th and 91st planetary harmonics as revealed in the photometry, ruling out the scenario of constructively phased and adequately modulated instrumental systematics.

We therefore conclude that the pulsations are stellar and not instrumental in nature, and we account for them by including two sine functions in the final version of our global fits. We find that the pulsations have respective amplitudes and frequencies of 35 ± 7 and 28 ± 6 ppm and 162.335 ± 0.015 and 186.976 ± 0.013 μHz —respectively, 79.006 ± 0.007 and 0.006 ± 0.007 times the orbital frequency.

3.5. HAT-P-2’s Radial Velocity

HAT-P-2’s RV measurements provide a complementary perspective to *Spitzer*’s. In addition to showing a high level of stellar jitter ($\sim 36 \text{ m s}^{-1}$; discussed in Section 4.2), the RV measurements suggest that HAT-P-2 b’s orbit is evolving in a way that is inconsistent with our previous fits to the photometry alone. Figure 5 shows that an independent analysis of the first half of HAT-P-2’s RV data (obtained prior to BJD 2454604) yields values for e and ω that are inconsistent at the 4.5σ level with those from a fit of the second half of the data (obtained

after BJD 2455466). This translates into respective variations of e and ω of $8.9 \pm 2.8E^{-4}$ and $0^\circ.91 \pm 0^\circ.31$ per year, which is inconsistent with the limits derived from the primary and secondary eclipse times alone.

4. Discussion

4.1. The Origin of HAT-P-2’s Pulsations

The exact correspondence of the stellar pulsation frequencies with harmonics of the planet’s orbital frequency implies a connection between the two. Two scenarios are possible; either the pulsations are altering the planet’s orbit or the planet is causing the pulsation. Mode-planet gravitational interactions could synchronize the planet’s orbital frequency to an integer harmonic of a mode oscillation period, analogous to two weakly coupled oscillators that synchronize in the presence of weak damping. However, the detection of multiple harmonics of the planet’s orbital frequency rules out this scenario.

We next consider the hypothesis that the observed stellar pulsations are induced by the orbiting planet. Tidally excited pulsations have been previously observed in several eccentric stellar binaries (Welsh et al. 2011; Thompson et al. 2012; Beck et al. 2014) known as “heartbeat” stars. The characteristic feature of a tidally excited pulsation is that its frequency is an exact integer harmonic of the orbital frequency because it arises from a resonantly forced stellar pulsation mode (Derekas et al. 2011; Burkart et al. 2012; Fuller & Lai 2012; O’Leary & Burkart 2014; Smullen & Kobulnicky 2015).

In order to understand the nature of the detected pulsations, we calculate the stellar response to tidal forcing. We first calculate the non-adiabatic stellar pulsation mode spectrum of HAT-P-2 using the MESA evolution code (Paxton et al. 2011, 2013) to describe the stellar evolution and the GYRE pulsation code (Townsend & Teitler 2013) to compute the pulsation modes. We then calculate the response of each pulsation mode to the tidal forcing and compute the amplitude and frequencies of each tidally excited pulsation. Our models indicate that although HAT-P-2 b can in principle create luminosity fluctuations of this amplitude in its host, we expect these pulsations to have much lower frequencies, in the vicinity of twice the periastron orbital frequency (Hut 1981)—approximately $10 \mu\text{Hz}$ (period of approximately 28 hr). Our models are unable to reproduce a tidally excited pulsation at the 79th or 91st orbital harmonics at the observed amplitude; the strength of the forcing at these harmonics is many orders of magnitude weaker than at the tidal forcing peak near the 6th orbital harmonic.

Although HAT-P-2 lies near the extreme cool ends of the γ -Doradus and δ -Scuti instability strips ($T_{\text{eff}} \sim 6300 \text{ K}$, $\log_{10} g \sim 4.16$, $R \sim 1.54 R_{\text{Sun}}$; Uytterhoeven et al. 2011; Balona et al. 2015), it shows no evidence of the large amplitude ($\sim \text{mmag}$) pulsations typically observed in these pulsators. Nonetheless, it is possible that the observed pulsations correspond to low-amplitude δ -Scuti pulsation modes, as our non-adiabatic pulsation calculations indicate that $l = 1$ and $l = 2$ pulsation modes are unstable near the observed frequencies of $f \sim 175 \mu\text{Hz}$, although we caution that mode growth rates—the parameter indicating stability of a pulsation mode—may be altered by a more realistic treatment of convective flux perturbations. In our models, the unstable modes correspond to low-order ($n < 3$) mixed pressure-gravity modes. In principle, these modes can couple strongly with HAT-P-2 b because they produce relatively large gravitational

²⁰ The PSF shape can be affected by structural changes of the instrument (e.g., due to heating).

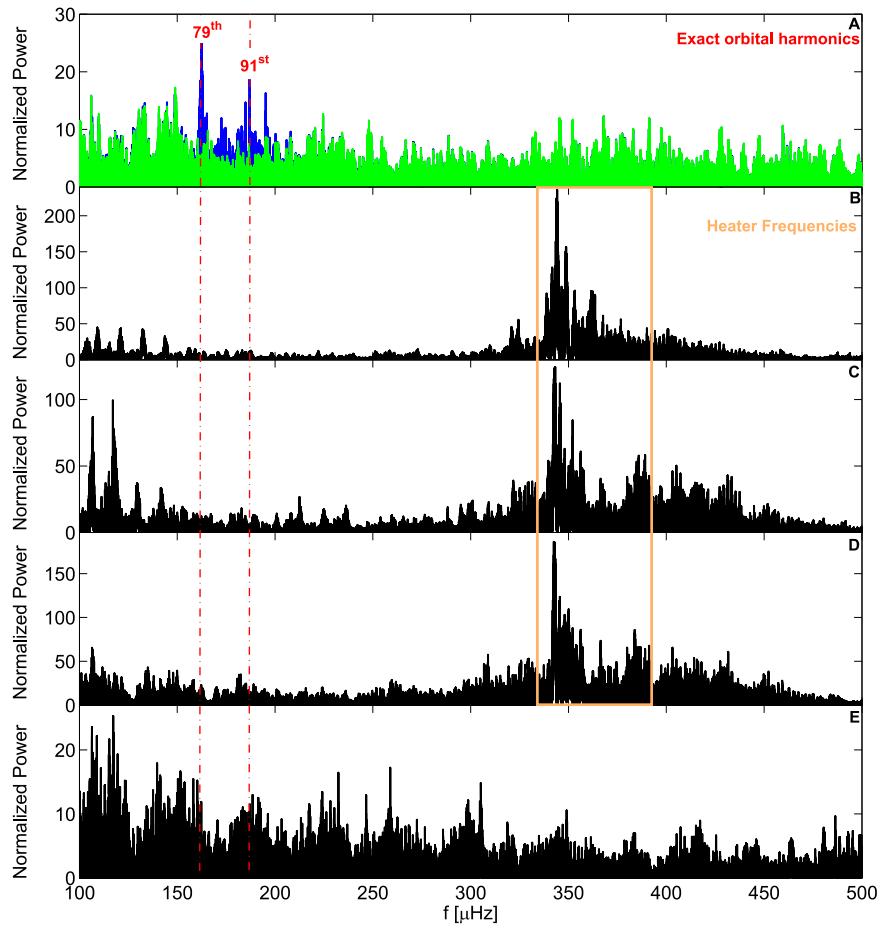


Figure 4. Periodogram of the 4.5 micron photometry compared to the periodograms of the point-spread function (PSF) change in position along x/y (B)/(C), the noise-pixel parameter (proxy for the PSF shape) (D), and the background contribution (E). No energy is found in at the frequency corresponding to the pulsation detected in HAT-P-2’s photometry ruling out their instrumental origin.

perturbations (i.e., they are similar to fundamental modes). However, our models suggest that they have frequencies that are too large to resonantly interact with the planet.

The failure of our models to explain the observed high-frequency pulsations suggests that current tidal theories may be incomplete. One tentative possibility is that nonlinear effects are important. The difference between the observed pulsations is $\simeq 12$ times the orbital frequency where resonant interactions with the planet can occur. This sort of nonlinear mode splitting at orbital harmonics has been observed in stellar systems (see, e.g., Hambleton et al. 2013) and could occur in the HAT-P-2 system as well.

4.2. Tidally Induced Pulsations and RV Measurements

Stellar pulsations cause RV variations of the stellar photosphere (e.g., Willems & Aerts 2002; Welsh et al. 2011). The RV amplitude of the photospheric motion due to a pressure mode is $\Delta v \sim 2\pi f \Delta R$, where ΔR is the mode surface displacement. Our non-adiabatic pulsation calculations indicate that the stellar surface displacements and luminosity variations are approximately related by $\Delta R/R \sim 2\Delta L/L$ for modes near the observed frequencies. The observed photometric amplitudes imply $\Delta v \sim 60 \text{ m s}^{-1}$, consistent with HAT-P-2’s large RV jitter. Mode identification would be required for a more precise calculation, but we posit that HAT-P-2’s RV jitter and

HAT-P-2 b’s apparent orbital evolution in the RV data is mainly produced by the pulsations.

5. Conclusion

Our study provides a new perspective on the planet–star interactions in HAT-P-2’s system. The extensive coverage of the system at $4.5 \mu\text{m}$ allows us to better disentangle the instrumental systematic from the planet’s transient heating, reconciling observations and atmospheric models. The photometric observations also show no sign of orbit-to-orbit variability nor of orbital evolution but reveals high-frequency low-amplitude stellar pulsations that correspond to harmonics of the planet’s orbital frequency, supporting their tidal origin. Current stellar models are however unable to reproduce these pulsations. HAT-P-2’s RV measurements exhibit a high level of jitter and support an orbital evolution of HAT-P-2 b inconsistent with the ultra-precise eclipse times. The inability of current stellar models to reproduce the observed pulsations and the exotic behavior of HAT-P-2’s RV indicate that additional observations and theoretical developments are required to understand the processes at play in this system.

Future missions such as *TESS*, *PLATO*, and *CHEOPS* will provide further insights into the nature of HAT-P-2’s pulsations and its interaction with its eccentric companion. The detection of multiple unexpected high-frequency pulsations as HAT-P-2’s could be used to indirectly hint at the presence of a companion—

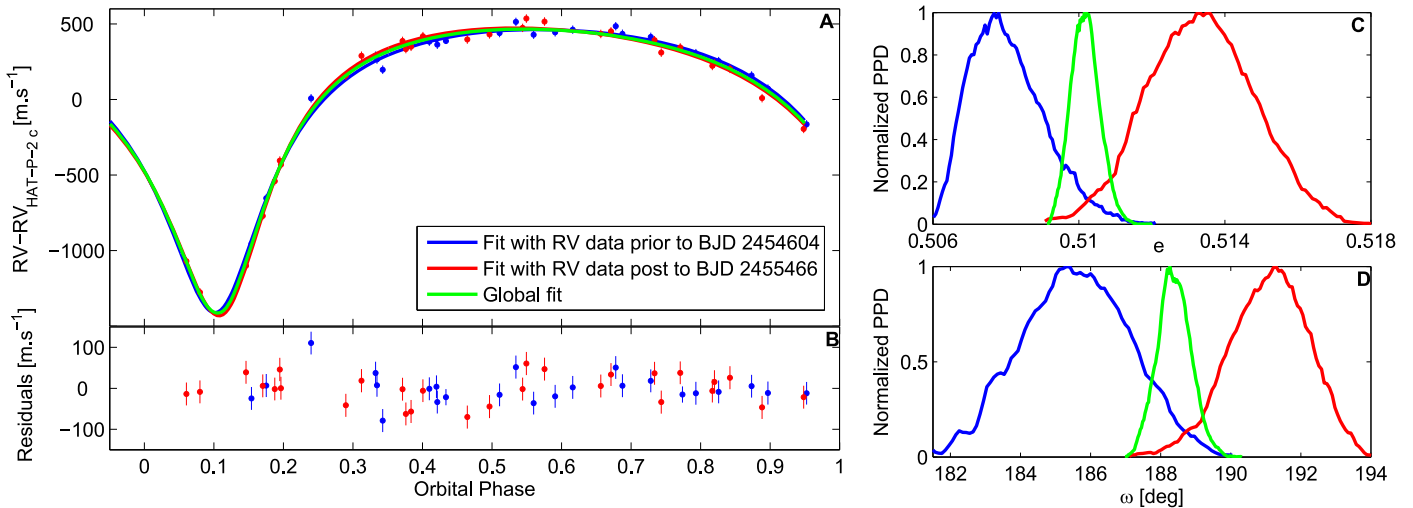


Figure 5. Complementary insights from HAT-P-2's radial velocity measurements. (A) HAT-P-2's RV measurement folded over HAT-P-2 b's period with long-term variation in the RV signal due to substellar object c removed. Measurements are shown as filled circles with their error bars and best fits as solid lines. Objects colored in green, blue, and red correspond respectively to quantities related to our global analysis, analysis using RV data prior to BJD 2454604, and analysis using RV data prior to BJD 245466. (B) Residuals of the RV fits. (C) Normalized posterior probability distribution (PPD) of HAT-P-2 b's orbital eccentricity. (D) Normalized PPD of HAT-P-2 b's periastron argument. The RV measurements show evidence of HAT-P-2 b's evolution at the 4.5σ level on e and ω , which is inconsistent with the insight gained from the ultra-precise eclipse times derived from *Spitzer*'s photometry.

regardless of their orbital inclination, to be later confirmed with traditional techniques such as direct imaging or RV.

This work is based on observations made with the *Spitzer Space Telescope*, which is operated by the Jet Propulsion Laboratory, California Institute of Technology, under contract to NASA. Support for this work was provided by JPL/Caltech. J.d.W. was further supported by the WBI (Wallonie-Bruxelles International) under the WBI-World Excellence Fellowship Program. A.S. performed this work in part under contract with the California Institute of Technology (Caltech) funded by NASA through the Sagan Fellowship Program executed by the NASA Exoplanet Science Institute. V.A. is funded by the Stellar Astrophysics Centre via the Danish National Research Foundation (grant DNR106). The research was supported by the ASTERISK project (ASTER-seismic Investigations with SONG and *Kepler*) funded by the European Research Council (grant agreement No. 267864). Radial velocity data presented herein were obtained at the W. M. Keck Observatory using time granted by the California Institute of Technology, UC Berkeley, and the University of Hawaii. We thank the observers who contributed to the measurements reported here and acknowledge the efforts of the Keck Observatory staff. We extend special thanks to those of Hawaiian ancestry on whose sacred mountain of Mauna Kea we are privileged to be guests.

J.d.W. thanks T. Rogers, V. Stamenković, A. Zsom, B.-O. Demory, M. Gillon, S. Seager, and V. Van Grootel for useful discussions during the preparation of this manuscript.

References

- Bakos, G. Á., Kovács, G., Torres, G., et al. 2007, *ApJ*, 670, 826
- Balona, L. A., Daszyńska-Daszkiewicz, J., & Pamyatnykh, A. A. 2015, *MNRAS*, 452, 3073
- Beck, P. G., Hambleton, K., Vos, J., et al. 2014, *A&A*, 564, A36
- Burkart, J., Quartaert, E., Arras, P., & Weinberg, N. N. 2012, *MNRAS*, 421, 983
- Cébron, D., Bars, M. L., Gal, P. L., et al. 2013, *Icar*, 226, 1642
- Cowan, N. B., & Agol, E. 2011, *ApJ*, 726, 82
- de Wit, J., Lewis, N., Langton, J., et al. 2016, *ApJL*, 820, L33
- Derekas, A., Kiss, L. L., Borkovits, T., et al. 2011, *Sci*, 332, 216
- Fabrycky, D. C., & Winn, J. N. 2009, *ApJ*, 696, 1230
- Fortney, J. J., Lodders, K., Marley, M. S., & Freedman, R. S. 2008, *ApJ*, 678, 1419
- Fuller, J., & Lai, D. 2012, *MNRAS*, 420, 3126
- Gillon, M., Lanotte, A. A., Barman, T., et al. 2010, *A&A*, 511, A3
- Hambleton, K. M., Kurtz, D. W., Prša, A., et al. 2013, *MNRAS*, 434, 925
- Hartman, J. D. 2010, *ApJL*, 717, L138
- Howard, A. W., Johnson, J. A., Marcy, G. W., et al. 2009, *ApJ*, 696, 75
- Hut, P. 1981, *A&A*, 99, 126
- Ingalls, J. G., Krick, J. E., Carey, S. J., et al. 2016, *AJ*, 152, 44
- Jordan, A., & Bakos, G. Á. 2008, *ApJ*, 685, 543
- Kataria, T., Showman, A. P., Lewis, N. K., et al. 2013, *ApJ*, 767, 76
- Langton, J., & Laughlin, G. 2008, *ApJ*, 674, 1106
- Levrard, B., Winisdoerffer, C., & Chabrier, G. 2009, *ApJL*, 692, L9
- Lewis, N. K., Knutson, H. A., Showman, A. P., et al. 2013, *ApJ*, 766, 95
- Lewis, N. K., Showman, A. P., Fortney, J. J., Knutson, H. A., & Marley, M. S. 2014, *ApJ*, 795, 150
- Mandel, K., & Agol, E. 2002, *ApJL*, 580, L171
- Mighell, K. J. 2005, *MNRAS*, 361, 861
- O'Leary, R. M., & Burkart, J. 2014, *MNRAS*, 440, 3036
- Paxton, B., Bildsten, L., Dotter, A., et al. 2011, *ApJS*, 192, 3
- Paxton, B., Cantiello, M., Arras, P., et al. 2013, *ApJS*, 208, 4
- Salz, M., Schneider, P. C., Czesla, S., & Schmitt, J. H. M. M. 2016, *A&A*, 585, L2
- Smullen, R. A., & Koblunicky, H. A. 2015, arXiv:1506.06196
- Stevenson, K. B., Harrington, J., Fortney, J. J., et al. 2012, *ApJ*, 754, 136
- Thompson, S. E., Everett, M., Mullally, F., et al. 2012, *ApJ*, 753, 86
- Townsend, R. H. D., & Teitler, S. A. 2013, *MNRAS*, 435, 3406
- Uytterhoeven, K., Moya, A., Grigahcène, A., et al. 2011, *A&A*, 534, A125
- Vogt, S. S., Allen, S. L., Bigelow, B. C., et al. 1994, *Proc. SPIE*, 2198, 362
- Welsh, W. F., Orosz, J. A., Aerts, C., et al. 2011, *ApJS*, 197, 4
- Willems, B., & Aerts, C. 2002, *A&A*, 384, 441
- Winn, J. N., Holman, M. J., Torres, G., et al. 2008, *ApJ*, 683, 1076
- Wong, I., Knutson, H. A., Kataria, T., et al. 2016, *ApJ*, 823, 122
- Wong, I., Knutson, H. A., Lewis, N. K., et al. 2015, *ApJ*, 811, 122